J. Fluid Mech. (2007), *vol.* 589, *pp.* 253–260.
doi:10.1017/S0022112007008014 Printed in the United Kingdom

Energy and enstrophy fluxes in the double cascade of two-dimensional turbulence

G. BOFFETTA

Dipartimento di Fisica Generale and INFN, Università degli Studi di Torino,
Via Pietro Giuria 1, 10125, Torino, Italy
and CNR-ISAC, Sezione di Torino, Corso Fiume 4, 10133 Torino, Italy

(Received 22 May 2007 and in revised form 11 July 2007)

High-resolution direct numerical simulations of two-dimensional turbulence in stationary conditions are presented. The development of an energy–enstrophy double cascade is investigated and its statistics found to be compatible with the classical Kraichnan theory in the limit of extended inertial ranges. The analysis of the joint distribution of energy and enstrophy fluxes in physical space reveals a small value of cross-correlation. This result supports many experimental and numerical studies where only one cascade is generated.

1. Introduction

The existence of two quadratic inviscid invariants is the most distinguishing feature of Navier–Stokes equations in two dimensions. On this basis, in a remarkable paper, Kraichnan (1967) predicted the double cascade scenario for two-dimensional turbulence: an inverse cascade of kinetic energy $E=(1/2)\langle v^2\rangle$ to large scales and a direct cascade of enstrophy $Z=(1/2)\langle\boldsymbol{\omega}^2\rangle$ to small scales ($\boldsymbol{\omega}=\nabla\times\boldsymbol{v}$ is the vorticity). In statistically stationary conditions, when the turbulent flow is sustained by an external forcing acting on a typical scale ℓ_f a double cascade develops. According to the Kraichnan theory, at large scales, i.e. wavenumbers $k\ll k_f\sim\ell_f^{-1}$, the energy spectrum has the form $E(k)\simeq\varepsilon^{2/3}k^{-5/3}$, while at small scales, $k\gg k_f$, the prediction is $E(k)\simeq\eta^{2/3}k^{-3}$, with a possible logarithmic correction (Kraichnan 1971). Here ε and $\eta\simeq k_f^2\varepsilon$ are respectively the energy and the enstrophy injection rate.

Despite the importance of two-dimensional turbulence as a model for many physical flows (see Kraichnan & Montgomery 1980; Tabeling 2002) and, more generally, for non-equilibrium statistical systems (Bernard *et al.* 2006), clear evidence of the two coexisting cascades on an extended range of scales is still lacking. The inverse energy cascade has been observed in many laboratory experiments, for example by Paret & Tabeling (1997), and in numerical simulations (see Siggia & Aref 1981; Frisch & Sulem 1984; Smith & Yakhot 1993; Borue 1994) with a statistical accuracy which has revealed the absence of intermittency corrections to dimensional scaling, as shown by Boffetta, Celani & Vergassola (2000). For the direct cascade, earlier numerical simulations, for example by Legras, Santangelo & Benzi (1988), and experiments (see Kellay, Wu & Goldburg 1995) report spectra slightly steeper than k^{-3}, while more recent investigations at higher resolution are closer to Kraichnan's prediction (Borue 1993; Gotoh 1998; Lindborg & Alvelius 2000; Pasquero & Falkovich 2002). It is important to note that Nam *et al.* (2000) have shown that in the presence of a large-scale drag force (always present in experiments and sometimes also in numerics)

Label	N	ν	α	ℓ_f/ℓ_d	$\varepsilon_\alpha/\varepsilon_I$	$\varepsilon_\nu/\varepsilon_I$	η_α/η_I	η_ν/η_I	T/τ_L
A	2048	2×10^{-5}	0.015	26.2	0.54	0.46	0.03	0.97	6.3
B	4096	5×10^{-6}	0.024	52.3	0.82	0.18	0.08	0.92	5.9
C	8192	2×10^{-6}	0.025	80.5	0.92	0.08	0.10	0.90	2.6
D	16384	1×10^{-6}	0.03	114.2	0.95	0.05	0.12	0.88	0.9

TABLE 1. Parameters of the simulations. N is spatial resolution, ν viscosity, α friction, L box size, $\ell_f = L/100$ forcing scale, $\ell_d = \nu^{1/2}/\eta_\nu^{1/6}$ enstrophy dissipative scale, ε_I energy injection rate, ε_ν viscous energy dissipation rate, ε_α friction energy dissipation rate, η_I enstrophy injection rate, η_ν viscous enstrophy dissipation rate, η_α friction enstrophy dissipation rate, T averaging time, $\tau_L = E/\varepsilon_\alpha$ large-scale eddy turnover time.

a correction to the classical exponent -3 is expected, clearly observed in simulations also by Boffetta *et al.* (2002).

Two recent experimental papers by Rutgers (1998) and Bruneau & Kellay (2005) have been devoted to the study of the double cascade. Their results are substantially consistent with the classical scenario of Kraichnan, although the extension of the inertial range (in particular for the inverse cascade) is limited and the flow is inhomogeneous at the scales of the inverse cascade. Here we present high-resolution (up to $16\,384^2$) direct numerical simulations of forced two-dimensional Navier–Stokes equations which reproduce with good accuracy both cascades simultaneously. Most of the injected energy flows to large scales (where it is removed by friction dumping) while enstrophy cascades to small scales (there removed by viscosity). We find strong numerical indications that the classical Kraichnan scenario is recovered in the limit of two extended inertial ranges, although we are unable to rule out, at the present resolution, the possibility of corrections to the direct cascade. By looking at the two fluxes in physical space, we find a relatively small value of the cross-correlation between them. This result suggests the possibility of generating a single cascade, independently of the presence of the second inertial range.

2. High-resolution direct numerical simulations

The two-dimensional Navier–Stokes equation for the vorticity field is

$$\partial_t \omega + \boldsymbol{v}\cdot\nabla\omega = \nu\Delta\omega - \alpha\omega + \Delta f, \tag{2.1}$$

where ν is the kinematic viscosity and α is a linear friction coefficient (representing bottom friction or air friction) necessary to obtain a stationary state. The forcing term f is assumed to be short correlated in time (in order to control the injection rates) and narrow banded in space. Specifically, we use a Gaussian forcing with correlation function $\langle f(\boldsymbol{r},t)f(\boldsymbol{0},0)\rangle = F\delta(t)\ell_f^2\exp(-(r/\ell_f)^2/2)$, where F is a constant, in most of the simulations. In order to check the independence of the results of the details of the forcing, for the simulations at resolution 16 384 we use a different forcing restricted to a narrow shell of wavenumbers. Numerical integration of (2.1) is performed by a pseudo-spectral, fully dealiased, parallel code on a doubly periodic square domain of side L at resolution N^2. After the system has reached a stationary state (i.e. constant value of kinetic energy), statistical quantities are computing by averaging over several large-scale eddy turnover times (only over a fraction of eddy turnover time for the 16 384 run because of limited resources). Table 1 reports the most important parameters of our simulations.

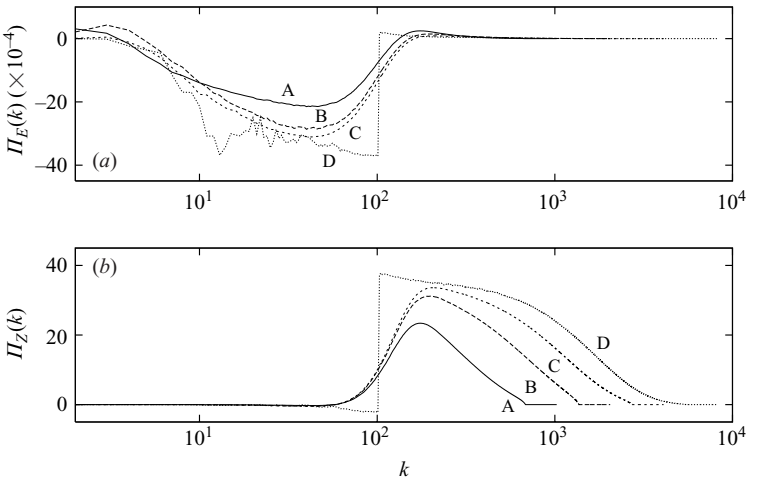

FIGURE 1. (*a*) Energy and (*b*) enstrophy fluxes in Fourier space at resolutions 2048 (A), 4096 (B), 8192 (C) and 16384 (D). At resolution 16384 fluxes are computed on a single frame.

One of the simplest pieces of information which can be obtained from table 1 is related to the energy–enstrophy balance. At $N = 2048$ only about half of the energy injected is transferred to large scales where it is removed by friction at a rate $\varepsilon_\alpha = 2\alpha E$. This fraction increases with the resolution and becomes about 95 % for the $N = 16386$ run. The remaining energy injected is dissipated by viscosity at scales comparable with the forcing scale and at a rate proportional to ν (which thus decreases on increasing the resolution).

Most of the enstrophy (around 90 %) follows the direct cascade to small scales, where it is dissipated by viscosity. We observe a moderate increase of the large-scale enstrophy dissipation η_α on increasing the resolution: this is a finite-size effect due the increase of α with N (see table 1) necessary to keep the friction scale $\ell_\alpha \simeq \varepsilon_\alpha^{1/2}\alpha^{-3/2}$ constant with increasing ε_α.

In figure 1 we plot the fluxes of energy and enstrophy in wavenumber space. Observe that because we change the resolution while keeping the ratio L/ℓ_f constant, the only effect of reducing the grid size on the inverse cascade is the decrease of the energy transferred to large scales (being $\varepsilon_\alpha = \varepsilon_I - \varepsilon_\nu$ with ε_ν proportional to ν) while the extent of the inertial range is almost unaffected. The behaviour of the fluxes around $k \simeq k_f$ depends on the details of the injection: the transition from zero to negative (positive) energy (enstrophy) flux is sharp in the case of forcing for a narrow band of wavenumber (run D) while it is more smooth for the Gaussian forcing which is active on more scales. Fluctuations observed in the energy flux for run D are a consequence of the short time statistics in this case. These results confirm the robustness of the energy inertial range regardless of the viscous dissipative scale, a further justification of many simulations of the inverse cascade in which, because of the limited resolution, the forcing scale is very close to the dissipative scale.

Unlike the inverse cascade, the direct enstrophy cascade is strongly affected by finite resolution effects. This is not a surprise because, by keeping ℓ_f fixed, the extent of the direct cascade is simply proportional to N. As shown in figure 1, we observe a range of wavenumbers with almost constant flux $\Pi_Z(k)$ only for the runs with $N \geqslant 8192$.

Figure 2 shows the energy spectra computed for the different runs. We remark again that the only effect of finite resolution on the inverse cascade is the reduction

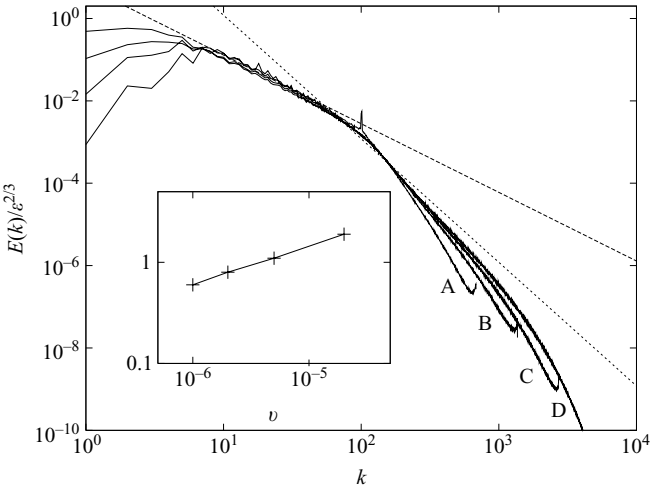

FIGURE 2. Energy spectra for the two simulations for the different resolutions (labels as in figure 1). Dashed and dotted lines represent the two predictions $Ck^{-5/3}$ with $C = 6$ and k^{-3} respectively. Inset: correction δ to the Kraichnan exponent -3 as a function of viscosity, computed by fitting the spectra with a power law $k^{-(3+\delta)}$ in the range $100 \leqslant k \leqslant 400$.

of the energy transferred to large scales, while the Kolmogorov scaling $k^{-5/3}$ is always observed with a Kolmogorov constant $C \simeq 6$, in agreement with Boffetta *et al.* (2000) and virtually independent of resolution. The effect of finite resolution on the enstrophy cascade range is, of course, more dramatic. We observe here a significant correction to the Kraichnan spectrum k^{-3} even for the 16 384 run, where we measure a scaling exponents close to -3.6. We note that a similar steepening of the spectrum has been observed even for simulations with a more resolved direct cascade range (here we have $k_{max}/k_f \simeq 55$ at the highest resolution). Despite these difficulties, there is a clear indication that the correction to the exponent is a finite-size effect which eventually disappears on increasing the extent of the inertial range (see inset of figure 2). The conclusion, therefore, is that a k^{-3} spectrum in stationary solutions of (2.1) could be achieved only by taking simultaneously the limits $L/\ell_f \to \infty$ and $\ell_f/\ell_d \to \infty$ (i.e. vanishing α and ν).

3. Analysis of fluxes in physical space

A better understanding of the physical mechanism at the basis of the cascades can be obtained by looking at the distribution of fluxes in space. This can be obtained by using a filtering procedure recently introduced and applied separately to the direct cascade by Chen *et al.* (2003) and to the inverse cascade by Chen *et al.* (2006). Thanks to the resolution of the present simulations, we are able to analyse both cascades jointly and also the correlation between them. Following Chen *et al.* (2003), we introduce a large-scale vorticity field $\omega_r \equiv G_r \star \omega$ obtained from the convolution of ω with a Gaussian filter G_r, and a large-scale velocity field $\boldsymbol{v}_r \equiv G_r \star \boldsymbol{v}$. From these definitions, balance equations for the large-scale energy $e_r(\boldsymbol{x}, t) = (1/2)|\boldsymbol{v}_r|^2$ and enstrophy $z_r(\boldsymbol{x}, t) = (1/2)\omega_r^2$ densities are easily written (with a compact notation):

$$\partial_t(e_r, z_r) + \nabla \cdot \boldsymbol{J}_r^{(e,r)} = -\Pi_r^{(e,r)} - D_r^{(e,r)} + F_r^{(e,r)} \tag{3.1}$$

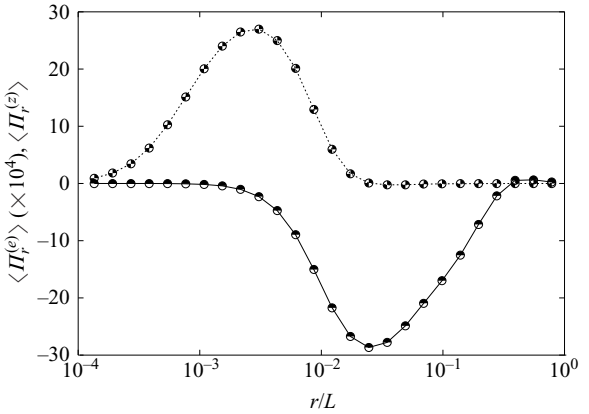

FIGURE 3. Average energy (lower, continuous) and enstrophy (upper, dotted) fluxes in physical space at resolution $N = 8192$. The energy flux is multiplied by a factor $k_f^2 = 10^4$ for better visualization.

where $\boldsymbol{J}_r^{(e,z)}$ represent the transport of large-scale energy and enstrophy, and $D_r^{(e,z)}$ and $F_r^{(e,r)}$ represent the large-scale dissipation and forcing. The energy/enstrophy fluxes $\Pi_r^{(e,z)}(\boldsymbol{x}, t)$, representing the local transfer of energy/enstrophy from large scale to scales smaller than r, are given by

$$\Pi_r^{(e)}(\boldsymbol{x}, t) \equiv -(\tau_{\alpha\beta})_r \nabla_\alpha (v_\beta)_r, \tag{3.2}$$

$$\Pi_r^{(z)}(\boldsymbol{x}, t) \equiv -(\sigma_\alpha)_r \nabla_\alpha \omega_r, \tag{3.3}$$

where $(\tau_{\alpha\beta})_r = (v_\alpha v_\beta)_r - (v_\alpha)_r (v_\beta)_r$ and $(\sigma_\alpha)_r = (v_\alpha \omega)_r - (v_\alpha)_r \omega_r$.

Fluxes (3.2) and (3.3) are expected to have a non-zero spatial mean in the inertial range of scales of irreversible turbulent cascades: in particular a mean negative energy flux for $r > \ell_f$ (inverse cascade) and a mean positive enstrophy flux for $r < \ell_f$ (direct cascade). Figure 3 shows the physical fluxes $\langle \Pi_r^{(e,z)} \rangle$ averaged over space and time, as functions of the scale r. The two cascades are evident although, as a consequence of the filtering procedure, the range of constant flux is apparently reduced with respect to the spectral case for both cascades (see figure 1).

Local fluxes are strongly inhomogeneous in physical space: there are relatively small regions of intense (positive and negative) flux in both the energy and enstrophy inertial ranges. Figure 4 shows two snapshots of the energy and enstrophy fluxes, computed from the same vorticity field at two different scales, $r_1 = 0.025L$ and $r_2 = 0.0025L$ corresponding to the minimum of energy flux and the maximum of enstrophy flux respectively (see figure 3). Interesting information, obtained from figure 4 at a qualitative level, is that the most intense energy and enstrophy fluxes appear in different physical regions without any apparent correlation.

Figure 4 shows that both positive and negative fluxes are observed: locally both energy and enstrophy can go to smaller or larger scales. In figure 5 the probability density function of the two fluxes is plotted. As observed in Chen *et al.* (2003, 2006), the shapes of the p.d.f.'s are nearly symmetric, confirming the qualitative picture inferred from figure 4. The mean value in both cases is the result of strong cancellations as its ratio with the standard deviation is -0.22 for the energy flux and 0.16 for the enstrophy flux. The skewness is also small, about -0.30 and 3.2 for the energy and enstrophy fluxes respectively.

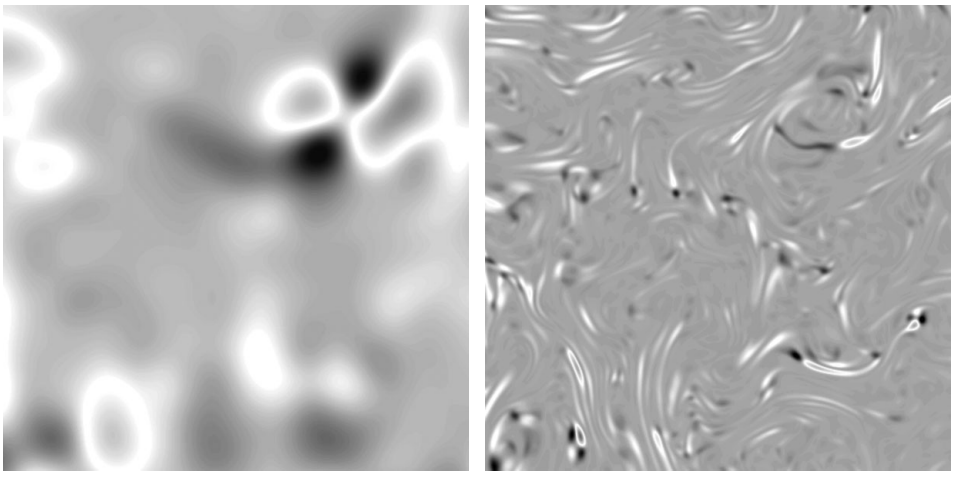

FIGURE 4. Snapshot of energy flux $\Pi_{r_1}^{(e)}$ (left) and enstrophy flux $\Pi_{r_2}^{(z)}$ (right) from the same vorticity field. Energy flux is computed at scale $r_1 = 0.025L$ and enstrophy flux at $r_2 = 0.0025L$, roughly corresponding to the minimum and maximum in figure 3. White and black correspond to positive and negative values respectively.

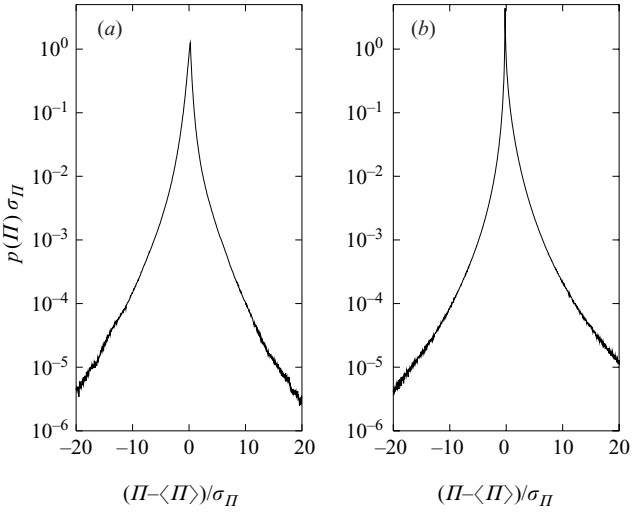

FIGURE 5. Probability density function of (*a*) energy $\Pi_{r_1}^{(e)}$ and (*b*) enstrophy $\Pi_{r_2}^{(z)}$ fluxes normalized with their standard deviations. Resolution is $N = 8192$, filtering scales are $r_1 = 0.025L$ and $r_2 = 0.0025L$.

Figure 6 shows the joint probability density function $p(\Pi_{r_1}^{(e)}, \Pi_{r_2}^{(z)})$ computed at the same scales r_1 and r_2 used in figure 4. This p.d.f. is not far from the product of the marginal distributions shown in figure 5, a condition for independence. Indeed, the correlation coefficient between $\Pi_{r_1}^{(e)}$ and $\Pi_{r_2}^{(z)}$ is only $C(r_1, r_2) \simeq -0.15$. Of course, it is very different if we consider the correlation at the same scale, for which we find $C(r_1, r_1) \simeq C(r_2, r_2) \simeq -0.9$ despite the fact that in this case one of the two fluxes has a mean close to zero. A possible interpretation of the observed small value of the correlation is the classical picture of independence of the two cascades, here obtained at a local level.

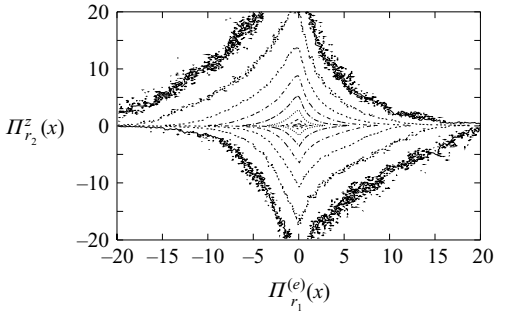

FIGURE 6. Joint probability density function $p(\Pi^{(e)}_{r_1}, \Pi^{(z)}_{r_2})$ of energy and enstrophy fluxes. Scales r_1 and r_2 as in figure 5. Contours are plotted on a logarithmic scale while fluxes are normalized with their standard deviations. Contour levels are (from outside to inside): 2.7×10^{-7}, 2.0×10^{-6}, 1.5×10^{-5}, 1.0×10^{-4}, 8.0×10^{-4}, 6.0×10^{-3}, 4.4×10^{-2}, 0.32.

4. Conclusions

In conclusion, we have presented a statistical analysis of high-resolution direct numerical simulations of two-dimensional Navier–Stokes equations. By increasing the resolution, most of the energy (enstrophy) flows to large (small) scales and the energy spectrum develops two power-law scaling ranges, in agreement with the double cascade scenario predicted by Kraichnan 40 years ago.

Simulations were performed on the IBM-CLX cluster of Cineca (Bologna, Italy) and on the *Turbofarm* cluster at the INFN computing centre in Torino.

REFERENCES

BERNARD, D., BOFFETTA, G., CELANI, A. & FALKOVICH, G. 2006 Conformal invariance in two-dimensional turbulence. *Nature Phys.* **2**, 124.

BOFFETTA, G., CELANI, A., MUSACCHIO, S. & VERGASSOLA, M. 2002 Intermittency in two-dimensional ekman-navier-stokes turbulence. *Phys. Rev.* E **66**, 026304.

BOFFETTA, G., CELANI, A. & VERGASSOLA, M. 2000 Inverse energy cascade in two-dimensional turbulence: Deviations from gaussian behavior. *Phys. Rev.* E **61**, R29.

BORUE, V. 1993 Spectral exponents of enstrophy cascade in stationary two-dimensional homogeneous turbulence. *Phys. Rev. Lett.* **71**, 3967.

BORUE, V. 1994 Inverse energy cascade in stationary two-dimensional homogeneous turbulence. *Phys. Rev. Lett.* **72**, 1475.

BRUNEAU, C. H. & KELLAY, H. 2005 Experiments and direct numerical simulations of two-dimensional turbulence. *Phys. Rev.* E **71**, 046305.

CHEN, S., ECKE, R. E., EYINK, G. L., RIVERA, M., WAN, M. & XIAO, Z. 2006 Physical mechanism of the two-dimensional inverse energy cascade. *Phys. Rev. Lett.* **96**, 084502.

CHEN, S., ECKE, R. E., EYINK, G. L., WANG, X. & XIAO, Z. 2003 Physical mechanism of the two-dimensional enstrophy cascade. *Phys. Rev. Lett.* **91**, 214501.

FRISCH, U. & SULEM, P. L. 1984 Numerical simulation of the inverse cascade in two-dimensional turbulence. *Phys. Fluids* **27**, 1921.

GOTOH, T. 1998 Energy spectrum in the inertial and dissipation ranges of two-dimensional steady turbulence. *Phys. Rev.* E **57**, 2984.

KELLAY, H., WU, X. L. & GOLDBURG, W. I. 1995 Experiments with turbulent soap films. *Phys. Rev. Lett.* **74**, 3975.

KRAICHNAN, R. H. 1967 Inertial ranges in two-dimensional turbulence. *Phys. Fluids* **10**, 1417.

KRAICHNAN, R. H. 1971 Inertial-range transfer in two- and three-dimensional turbulence. *J. Fluid Mech.* **47**, 525.

Kraichnan, R. H. & Montgomery, D. 1980 Two-dimensional turbulence. *Rep. Prog. Phys.* **43**, 547.

Legras, B., Santangelo, P. & Benzi, R. 1988 High-resolution numerical experiments for forced two-dimensional turbulence. *Europhys. Lett.* **5**, 37.

Lindborg, E. & Alvelius, K. 2000 The kinetic energy spectrum of the two-dimensional enstrophy turbulence cascade. *Phys. Fluids* **12**, 945.

Nam, K., Ott, E., Antonsen, T. M. & Guzdar, P. N. 2000 Lagrangian chaos and the effect of drag on the enstrophy cascade in two-dimensional turbulence. *Phys. Rev. Lett.* **84**, 5134.

Paret, J. & Tabeling, P. 1997 Experimental observation of the two-dimensional inverse energy cascade. *Phys. Rev. Lett.* **79**, 4162.

Pasquero, C. & Falkovich, G. 2002 Stationary spectrum of vorticity cascade in two-dimensional turbulence. *Phys. Rev.* E **65**, 056305.

Rutgers, M. A. 1998 Forced 2d turbulence: Experimental evidence of simultaneous inverse energy and forward enstrophy cascades. *Phys. Rev. Lett.* **81**, 2244.

Siggia, E. & Aref, H. 1981 Point-vortex simulation of the inverse energy cascade in two-dimensional turbulence. *Phys. Fluids* **24**, 171.

Smith, L. & Yakhot, V. 1993 Bose condensation and small-scale structure generation in a random force driven 2d turbulence. *Phys. Rev. Lett.* **71**, 352.

Tabeling, P. 2002 Two-dimensional turbulence: a physicist approach. *Phys. Rep.* **362**, 1.